ACS OMEGA

http://pubs.acs.org/journal/acsodf

Article

Antidegradation Property of Alginate Materials by Riveting Functionalized Carbon Nanotubes on the Sugar Chain

Zhenjie Jiang, Xuchao Wang, Xiaojing Long,* Zhihui Zhao,* and Yanzhi Xia*

Cite This: *ACS Omega* 2021, 6, 12813−12819

Read Online

ACCESS | Metrics & More | Article Recommendations | Supporting Information

ABSTRACT: Alginate materials with the advantages of being renewable, inexpensive, and environment-friendly have been considered promising fiber materials. However, they are prone to degrade under UV light, limiting their large-scale application in the textile field. Herein, the fracture of glycosidic bonds during the degradation process is revealed clearly by Fourier transform infrared (FT-IR) and ^{1}H NMR. To effectively inhibit this process, functionalized multiwalled carbon nanotubes (MWCNTs) are chosen as dopants and used to interact with the sugar chain via hydrogen bonds. The results demonstrate that alginate materials with functionalized MWCNTs exhibit slower degradation rates. The intermolecular energy transfer between functionalized MWCNTs and sodium alginate (SA) is proposed for the antidegradation effect of functionalized MWCNTs, which is supported by the experiments. Moreover, SA/MWCNT fibers also show enhanced mechanical properties compared with pure alginate fibers. The appealing effect of the degradation inhibition feature makes the composite alginate materials very promising candidates for their future use in textile material development.

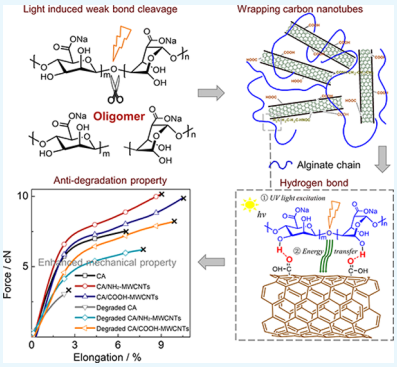

1. INTRODUCTION

Nowadays, alginate fibers are considered as one of the most promising alternative fibrous materials due to their superior properties, such as biocompatibility, intrinsic flame retardancy, radioresistance, antibacterial properties, etc.[1−8] Alginate, composed of a (1−4)-linked β-D-mannuronic acid (M) block and α-L-guluronic acid (G) blocks with a random arrangement in the backbone, is an important component of these fibrous materials.[9−17] However, alginate alginate macromolecules are easy to degrade in the presence of sunlight and microorganisms, which has a great impact on the spinning technology. Generally, degradation of natural polymers can be an undesirable or desirable process depending on their application fields. For example, natural polymer plastics and pesticides should be used as environmentally friendly products and the degradation process is permitted. While strength and flexibility properties are the prerequisite for natural polymer fibers, the degradation process is detrimental to their commercial applications and should be prevented.[18,19] Therefore, for the rapid development of the natural polymer textile industry, the degradation of alginate materials should be inhibited. Also, the degradation mechanism needs to be studied intensively.

Many strategies have been employed to inhibit the degradation of alginate materials. Metal ions have been successfully applied to cross-link alginate chains; the degradation of these ionically cross-linked alginate aqueous solutions could be inhibited effectively.[20−25] Unfortunately, the cross-linked alginate solutions lack flowability, which are difficult to process further. In comparison, the reinforcement of a secondary phase is an alternative method to avoid their rapid degradation in the ambient environment and maintain favorable processibility of the alginate solutions.[26−29] Among these materials, multiwalled carbon nanotubes (MWCNTs) show good biocompatibility, excellent electrical conductivity, and advanced mechanical properties. They are widely used in the fields of electronics and textiles.[30−38] Studies also suggest that MWCNTs can adsorb bacteria and exhibit strong antibacterial properties.[39] Generally, to make the original MWCNTs soluble in aqueous solutions, water-soluble groups are needed to be introduced on the MWCNTs. In addition, the substituted groups would also contribute to form hydrogen bonds between alginate and MWCNTs via the O−H···O interaction.[40] Thus, the MWCNTs can effectively prevent the degradation of the alginate polymer framework. However, the details about the antidegradation and the corresponding mechanism are not involved.

In this article, alginate materials show inhibited degradation rates by encapsulating COOH- or NH_2-functionalized MWCNTs. Compared to pure alginate materials, SA/MWCNTs show slower degradation rates with their degradation rate constants of 0.57×10^{-4} and 2.44×10^{-4}

Received: March 3, 2021
Accepted: April 29, 2021
Published: May 7, 2021

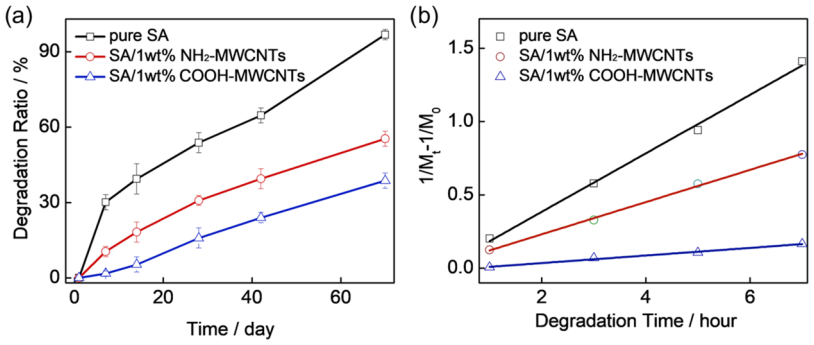

Figure 1. (a) Degradation ratio of SA and its composite solutions under sunlight. (b) Degradation rate constant of SA and its composite solutions under 365 nm UV irradiation.

h^{-1} for SA/COOH-MWCNTs and SA/NH_2-MWCNTs, respectively (Figure 1). Moreover, these SA/MWCNT fibers endow enhanced tensile modulus and strength. All these results indicate that MWCNTs significantly inhibit the degradation of alginate materials. Fourier transform infrared (FT-IR) (Figure 2) and ^{1}H NMR spectra data indicate that

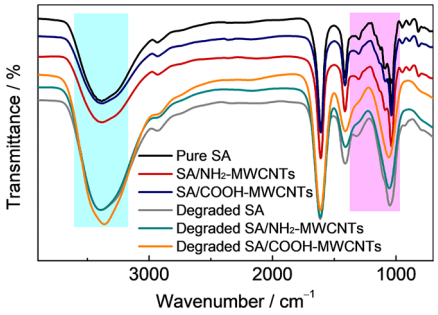

Figure 2. FT-IR spectra of pure SA as well as SA/NH_2-MWCNTs and SA/COOH-MWCNTs composites before and after degradation.

only the sensitive glycosidic bond in the backbone of alginate is broken and other chemical structures in the main chain are reserved. Based on the fluorescence spectra, the functionalized MWCNTs are used as energy acceptors, which can take the high energy away from the UV-excited SA macromolecule and stabilize the SA chemical structure (Figure 3). It is well concluded that the entire path of the degradation decreases by controlling this step of degradation. The antidegradation results are mainly ascribed to the bound hydrogen bonds and the resulting intermolecular energy transfer between alginate and MWCNTs.

2. RESULTS AND DISCUSSION

The cleavage of glycosidic bonds in the backbone has a great impact on the molecular weight of sodium alginate molecules. Therefore, gel permeation chromatography (GPC) and a Ubbelohde capillary viscometer are used, and the measured number average molecular weight (M_n), polydispersity index (PDI), and intrinsic viscosity ([η]) are listed in Table 1. After 24 days of illumination, the degraded SA/MWCNTs exhibit higher M_n (154 and 121 kDa) and [η] (6.9 dL/g and 6.0 dL/g) as well as narrower distribution (PDI = 1.62 and 1.72) than the degraded SA with lower M_n (65 kDa) and [η] (4.1 dL/g) and broader distribution (PDI = 1.86).

The degradation behaviors under sunlight are further evaluated and the results are shown in Figure 1a. The degradation rate of the pure SA solution is much larger than that of SA/MWCNTs, and the SA/COOH-MWCNTs composite shows the slowest degradation process. Moreover, their degradation kinetics is studied in the accelerated degradation process with 365 nm UV radiation. Figure 1b is plotted according to the equation $1/M_t - 1/M_0 = kt/m$. In this equation, M_t and M_0 are the viscosity average molecular weights of alginate macromolecules at different times, k is the rate constant, and m is the molecular weight of the alginate monomer.[41] All samples show linear correlations, indicating the first-order degradation kinetic reaction. The rate constant and half-life are calculated and listed in Table 2. Compared to pure SA, the composites exhibit smaller rate constants and longer half-lives, which also indicates that functionalized MWCNTs could effectively inhibit the degradation of SA under UV light.

FT-IR spectra are employed to confirm the variation of SA before and after degradation. As shown in Figure 2, the strong adsorption of 3390 cm^{-1} is attributed to the stretching of hydroxyl groups. Compared with undegraded materials, the peaks of degraded samples at 3390 cm^{-1} become stronger and broader. The result indicates that the degradation happens at the position of glycosidic bonds and numerous additional hydroxyl groups are formed. In addition, the spectra of degraded samples exhibit most of the characteristic adsorption peaks of the undegraded counterparts, but some tiny differences can be observed. The −C−OH stretching vibrations of degraded SA/NH_2-MWCNTs and SA/COOH-MWCNTs composites at 1061 cm^{-1} are shifted to a low energy region of ca. 20 cm^{-1} compared to that of pure SA, which is due to the interactions of −OH groups of SA and −C═O/−NH_2 groups of MWCNTs.

According to Petro Lutsyk's report,[42] MWCNTs can serve as energy acceptors. As shown in the UV−vis absorption spectra (Figure 3a), SA has no obvious absorption peak (Figure S2), while the SA/COOH-MWCNTs composite exhibits slightly higher intensities at 250 and 300 nm than those of COOH-MWCNTs, which is attributed to the contribution of the weak absorption of SA. To verify the intermolecular energy transfer process of SA/MWCNTs composites, their fluorescence spectra under the same concentration are measured with SA and MWCNTs as control (Figure 3b). The emission curves at 350 and 500 nm are chosen for comparison, as the former is mainly attributed to SA and the latter mainly belongs to MWCNTs. Compared to SA and COOH-MWCNTs, the emission of the SA component (350 nm) has decreased in the mixture system, while that of the MWCNTs component (500 nm) is enhanced. The

https://doi.org/10.1021/acsomega.1c01159
ACS Omega 2021, 6, 12813−12819

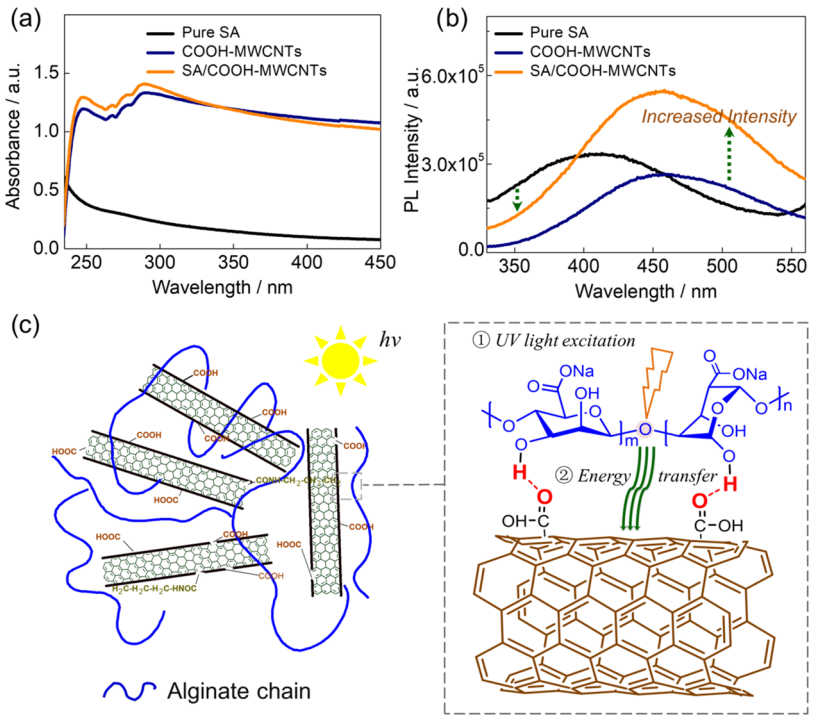

Figure 3. (a) UV−vis absorption and (b) fluorescence spectra of pure SA, COOH-MWCNTs, and the composite in aqueous solution. (c) Schematic diagram of the SA/MWCNTs composite and the energy transfer process in the SA/MWCNTs composite.

Table 1. $[\eta]$, M_W, M_n, and PDI of Alginate and Its Composite Solutions before and after Degradation

	$[\eta]$ (dL/g)	M_W (kDa)	M_n (kDa)	PDI
pure SA	8.2	325	224	1.45
degraded SA[a]	4.1	109	65	1.86
degraded SA/COOH-MWCNTs[a]	6.9	249	154	1.62
degraded SA/NH_2-MWCNTs[a]	6.0	208	121	1.72

[a]Degraded for 24 days.

Table 2. Rate Constant (k) and Half-Life ($t_{1/2}$) of SA, SA/NH_2-MWCNTs, and SA/COOH-MWCNTs

	rate constant ($\times 10^{-6}$)	$t_{1/2}$ (day)
SA	437	70
SA/NH_2-MWCNTs	244	116
SA/COOH-MWCNTs	57.4	519

phenomenon supports the energy transfer process from SA to MWCNTs in the SA/COOH-MWCNTs composite. Similar results can also be found in the SA/NH_2-MWCNTs system (Figure S3). Thus, the ultraviolet energy absorbed by alginate macromolecules can be transferred to MWCNTs, which is supposed to suppress the cleavage of glycosidic bonds in SA chains and beneficial to stabilize the molecular structure of SA under ultraviolet light (Figure 3c).

The polymer microstructures with and without MWCNTs are also determined by ^{1}H NMR spectra. The additional peaks of degraded SA with the chemical shifts in a low-field regime are dependent on the chemical identity of neighboring residues. Thus, multiple peaks for the protons in monosaccharide, disaccharide (MM, MG, GM, and GG), and trisaccharide (GGG, GGM, MGG, and MGM) segments are observed.[43] As shown in Figure 4b, the proton peaks at 5.2−6.0 ppm for pure SA present the produced oligomers after irradiation (Figure 4a). The anomeric protons at δ = 5.04 ppm

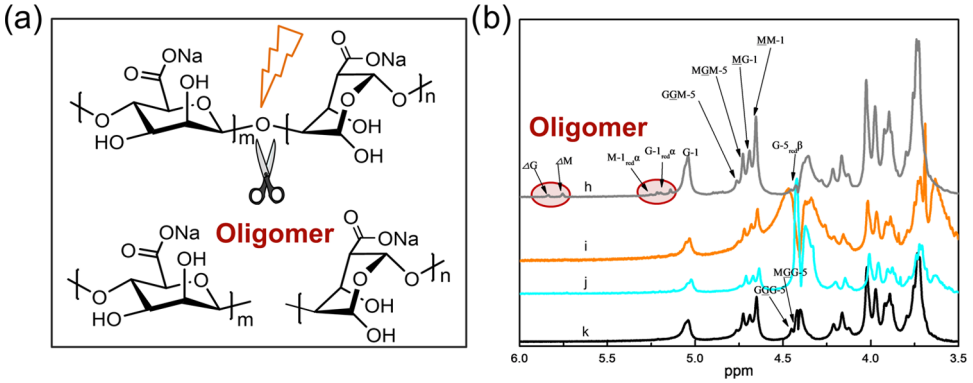

Figure 4. (a) Cleavage of the glycosidic bonds and the resulting oligomers under UV irradiation. (b) ^{1}H NMR spectra of degraded SA (h), degraded SA/COOH-MWCNTs (i), degraded SA/NH_2-MWCNTs (j), and pure SA (k).

https://doi.org/10.1021/acsomega.1c01159
ACS Omega 2021, 6, 12813−12819

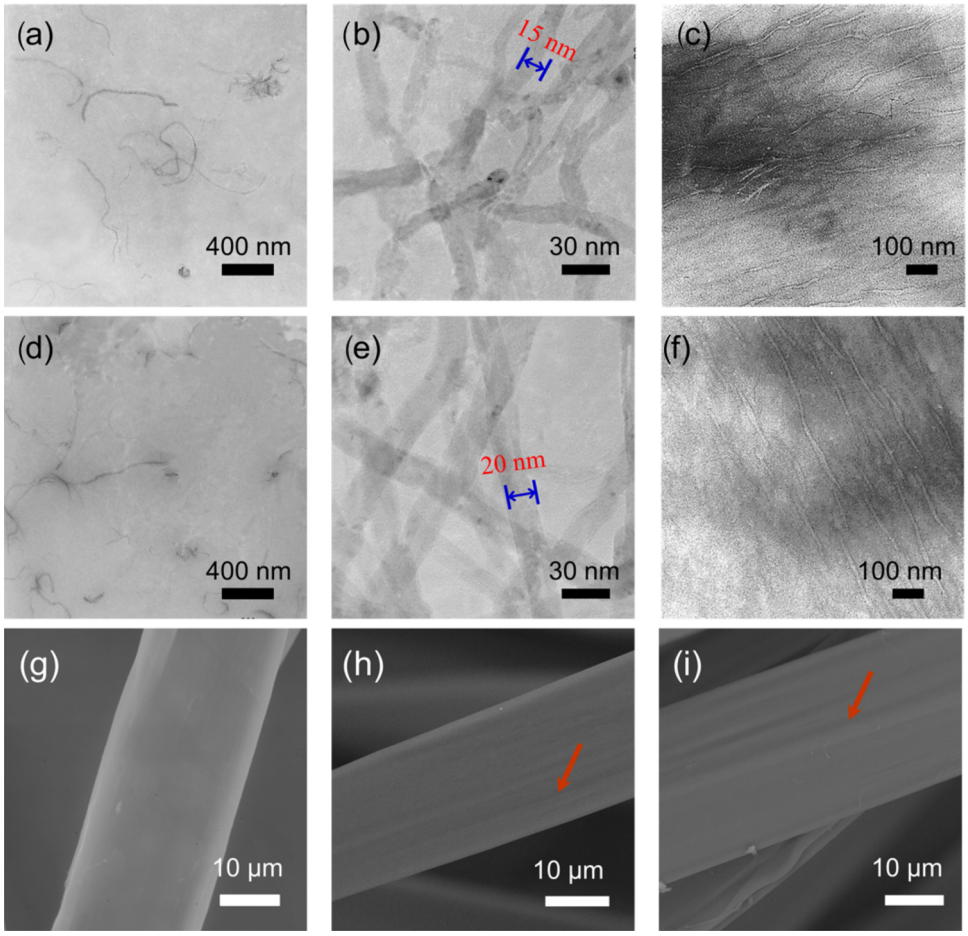

Figure 5. TEM images of COOH-MWCNTs (a–c) and NH_2-MWCNTs (d–f) in aqueous solutions (a, d), alginate solutions (b, e), and alginate fibers (c, f). SEM images of pristine CA (g), CA/COOH-MWCNTs (h), and CA/NH_2-MWCNTs (i).

come from guluronate residues. The overlapping peaks ranging from 4.76 to 4.64 are GGM, MGM, MG, and MM signals. Combining the FT-IR and ^{1}H NMR results, it can be concluded that the degradation happens at the position of the glycosidic bonds and results in additional hydroxyl groups.

Figure 5 shows the scanning electron microscopy (SEM) and transmission electron microscopy (TEM) images of the dispersibility of functional MWCNTs in different states. As observed in Figure 5a,d, both NH_2-MWCNTs and COOH-MWCNTs are uniformly dispersed in aqueous solutions through ultrasonication. The diameter of the MWCNTs is between 10 and 25 nm (Figure 5b,e). Moreover, MWCNTs can be observed in the longitudinal section of alginate composite fibers, resulting in a much higher degree of tube arrangement. The ordered orientation of MWCNTs in the fibers is very desirable for its application in textiles. Figure 5g–i shows the SEM images of pure calcium alginate fibers (CA) and CA/MWCNTs composite fibers. The surface morphology of pure CA fiber displays a smooth structure (Figure 5g), while those fibers with MWCNTs reveal a rather rough morphology with salient banded structures (Figure 5h,i). The results show that MWCNTs affect the morphology of these fibers.

As the inhibited degradation of SA/MWCNTs is promising in alginate fibers, the corresponding fibers are prepared from their solutions with and without one month's degradation. Representative stress–elongation curves of the fibers are presented in Figure 6. The pristine CA and its composite

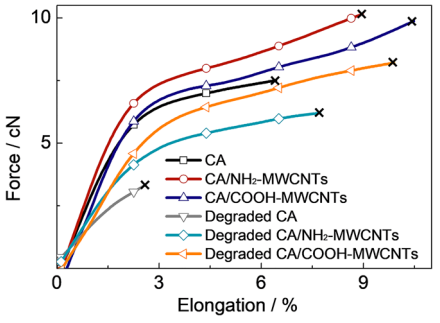

Figure 6. Stress–elongation graphs of CA as well as CA/NH_2-MWCNTs and CA/COOH-MWCNTs composites before and after degradation.

fibers exhibit higher breaking strength, elongation, and tensile modulus than that of the degraded counterparts. Moreover, the fibers loaded with nanotubes exhibit enhanced tensile strength. Therefore, the CA/MWCNT fibers exhibit higher mechanical properties than pristine CA fibers, which is consistent with the ordered orientation of MWCNTs in TEM images. However, the degraded CA/MWCNT fibers exhibit much higher mechanical properties than the degraded CA fibers, demonstrating the excellent antidegradation effect of MWCNTs. In addition, compared to pristine CA fibers, CA/COOH-MWCNTs and CA/NH_2-MWCNTs show higher limit oxygen index (LOI) values of 41 and 40%, respectively (Figure S4). It

https://doi.org/10.1021/acsomega.1c01159
ACS Omega 2021, 6, 12813–12819

is noteworthy that the functionalized MWCNTs have improved the flame retardant effect of alginate materials. These results indicate that MWCNTs are effective additives to inhibit the degradation of alginate materials. Moreover, they endow the materials with potential excellent properties.

3. CONCLUSIONS

In summary, we have studied the degradation inhibition measure of alginate materials. The results show that the backbone cleavages of the materials happen on glycosidic bonds and the resulting oligomers promote their degradation further. As an efficient degradation inhibition phase, MWCNTs are added into the system. The excellent properties of MWCNTs endow the alginate materials with a mitigated degradation process and improved tensile strength. We have also studied the potential degradation inhibition mechanism. It shows that MWCNTs can form hydrogen bonds with alginate macromolecules, and the intermolecular energy transfer can suppress the cleavage of glycosidic bonds. These results suggest that MWCNTs are promising additives to endow the alginate materials with inhibited degradation and superior properties.

4. EXPERIMENTAL SECTION

4.1. Materials. Multiwalled carbon nanotubes (MWCNTs) that include amine-modified (NH_2−) and carboxyl-modified (COOH−) multiwalled carbon nanotubes were provided by Chengdu Organic Chemicals Co., Ltd., Chinese Academy of Science (Chengdu, China). Calcium chloride anhydrous ($CaCl_2$) was purchased from Sinopharm Chemical Reagent (Shanghai, China). Sodium alginate (M_w = 296 kDa, PDI = 1.24) was purchased from the Hyzlin Biology Development Co., Ltd. (Qingdao, China). All of them were used without further purification.

4.2. Preparation of Materials. Sodium alginate (SA) with 1% NH_2-MWCNTs or COOH-MWCNTs were dissolved into deionized water and their aqueous solutions were formed, separately. After vigorously stirred for 3 h, 5 wt % pure and composite sodium alginate solutions were prepared to form aqueous solutions of SA, SA/COOH-MWCNTs, and SA/NH_2-MWCNTs. The solutions were extruded from a spinneret into a coagulating bath with a 5% calcium chloride aqueous solution, forming calcium alginate (CA), CA/COOH-MWCNT, and CA/NH_2-MWCNT fibers.

4.3. Characterization. Nuclear magnetic resonance (^{1}H NMR) spectra were measured with a Bruker AV-600 in D_2O at 60 °C. The chemical shift is reported in δ ppm using D_2O (4.79 ppm). UV−vis absorption spectra were recorded with a Shimadzu UV-3600 spectrometer. Fluorescence spectra were recorded with a Hitachi F-4500 spectrometer in spectral grade solvents. Infrared spectra were obtained using a Thermo Nicolet 5700 Fourier transform infrared spectrometer (FT-IR) with a resolution of 8 cm^{-1}. The limit oxygen index test was carried out using an oxygen indexer (LOI HC-2). Thermal analyses were performed using differential scanning calorimetry (DSC 822e) under a nitrogen flow at a heating rate of 10 °C min^{-1}. The scanning electron microscopy (JEOL Co., Japan) images were obtained with a JSM-840. The transmission electron microscopy (TEM) images were obtained with a JEM-1200 (JEOL Co., Japan) operated at an accelerating voltage of 100 kV. The molecular weights of the polymers were determined by gel permeation chromatography (GPC) on a Viscotek TDA 302-type at a temperature of 35 °C. The viscosity average molecular weight (M_η) was calculated from intrinsic viscosities $[\eta]$ measured by a Ubbelohde capillary viscometer. The apparent viscosities were determined by a Brookfield DV−II + programmable viscometer (Brookfield Engineering Labs, Inc.).

The degradation ratio of the alginate solution was calculated employing the equation of the degradation ratio (%) = $[(X - Y)/X] \times 100$, where X is the initial apparent viscosity of the alginate solution and Y is the detected viscosity. Then, M_η was determined from the intrinsic viscosity of a 0.1 mol/L NaCl solution and 0.05% EDTA-2Na at 20 ± 0.05 °C. Under these conditions, the Mark−Houwink equation for sodium alginate is: $[\eta] = K \times M_\eta^{\alpha}$ ($K = 2.0 \times 10^{-5}$, $\alpha = 1$).

4.4. Tensile Measurements. The CA, CA/COOH-MWCNT, and CA/NH_2-MWCNT fibers were tested using an Instron Tensile Testing Instrument. The breaking strength, elongation, and tensile modulus were calculated from the relative data to evaluate the effect of degradation on their mechanical properties.

■ ASSOCIATED CONTENT

Supporting Information

The Supporting Information is available free of charge at https://pubs.acs.org/doi/10.1021/acsomega.1c01159.

TGA curves of SA, SA/COOH-CNTs, and SA/NH_2-CNTs; UV−vis absorption of SA with different degradation times; fluorescence spectra of pure SA, NH_2-MWCNTs, and the composite in aqueous solution; and LOI and combustion parameter of pristine CA, CA/COOH-MWCNTs, and CA/NH_2-MWCNTs (PDF)

■ AUTHOR INFORMATION

Corresponding Authors

Xiaojing Long − *State Key Laboratory of Bio-Fibers and Eco-Textiles, Shandong Collaborative Innovation Center of Marine Biobased Fibers and Ecological Textiles, Institute of Marine Biobased Materials, College of Materials Science and Engineering, Qingdao University, Qingdao 266071, P. R. China*; orcid.org/0000-0002-9899-1820; Email: longxj@qdu.edu.cn

Zhihui Zhao − *State Key Laboratory of Bio-Fibers and Eco-Textiles, Shandong Collaborative Innovation Center of Marine Biobased Fibers and Ecological Textiles, Institute of Marine Biobased Materials, College of Materials Science and Engineering, Qingdao University, Qingdao 266071, P. R. China*; Email: zzh@qdu.edu.cn

Yanzhi Xia − *State Key Laboratory of Bio-Fibers and Eco-Textiles, Shandong Collaborative Innovation Center of Marine Biobased Fibers and Ecological Textiles, Institute of Marine Biobased Materials, College of Materials Science and Engineering, Qingdao University, Qingdao 266071, P. R. China*; Email: xiayz@qdu.edu.cn

Authors

Zhenjie Jiang − *State Key Laboratory of Bio-Fibers and Eco-Textiles, Shandong Collaborative Innovation Center of Marine Biobased Fibers and Ecological Textiles, Institute of Marine Biobased Materials, College of Materials Science and Engineering, Qingdao University, Qingdao 266071, P. R. China*

https://doi.org/10.1021/acsomega.1c01159
ACS Omega 2021, 6, 12813−12819

Xuchao Wang − *Department of Environmental and Chemical Engineering, Tangshan University, Tangshan 063000, P. R. China*

Complete contact information is available at: https://pubs.acs.org/10.1021/acsomega.1c01159

Notes

The authors declare no competing financial interest.

■ ACKNOWLEDGMENTS

The authors are grateful for financial support from the Postdoctoral Science Foundation of China (Nos. 2018M640610 and 2019T120570), the Natural Science Foundation of Shandong Province (ZR2019BEM016), the Taishan Scholars Program (No. tsqn201909090). The authors also acknowledge support from the State Key Laboratory of Bio-Fibers and Eco-Textiles, Qingdao University (No. ZKT06 and GZRC202008), and the test center of Tangshan Graphene Application Technology Public Service Platform.

■ REFERENCES

(1) Abu-Rabeah, K.; Polyak, B.; Ionescu, R. E.; Cosnier, S.; Marks, R. S. Synthesis and characterization of a pyrrole-alginate conjugate and its application in a biosensor construction. *Biomacromolecules* **2005**, *6*, 3313−3318.

(2) Webber, R. E.; Shull, K. R. Strain dependence of the viscoelastic properties of alginate hydrogels. *Macromolecules* **2004**, *37*, 6153−6160.

(3) Kovalenko, I.; Zdyrko, B.; Magasinski, A.; Hertzberg, B.; Milicev, Z.; Burtovyy, R.; Luzinov, L.; Yushin, G. A major constituent of brown algae for use in high-capacity Li-ion batteries. *Science* **2011**, *334*, 75−79.

(4) Pawar, S. N.; Edgar, K. J. Alginate derivatization: a review of chemistry, properties and applications. *Biomaterials* **2012**, *33*, 3279−3305.

(5) Park, H. R.; Jung, K. A.; Lim, S.-R.; Park, J. M. Quantitative sustainability assessment of seaweed biomass as bioethanol feedstock. *BioEnergy Res.* **2014**, *7*, 974−985.

(6) Yong, Y.-C.; Liao, Z.-H.; Sun, J.-Z.; Zheng, T.; Jiang, R.-R.; Song, H. Enhancement of coulombic efficiency and salt tolerance in microbial fuel cells by graphite/alginate granules immobilization of *Shewanella oneidensis* MR-1. *Process Biochem.* **2013**, *48*, 1947−1951.

(7) George, M.; Abraham, T. E. Polyionic hydrocolloids for the intestinal delivery of protein drugs: Alginate and chitosan-a review. *J. Controlled Release* **2006**, *114*, 1−14.

(8) Chan, A. W.; Neufeld, R. J. Tuneable semi-synthetic network alginate for absorptive encapsulation and controlled release of protein therapeutics. *Biomaterials* **2010**, *31*, 9040−9047.

(9) Papageorgiou, S. K.; Kouvelos, E. P.; Favvas, E. P.; Sapalidis, A. A.; Romanos, G. E.; Katsaros, F. K. Metal-carboxylate interactions in metal-alginate complexes studied with FTIR spectroscopy. *Carbohydr. Res.* **2010**, *345*, 469−473.

(10) Marrella, A.; Lagazzo, A.; Barberis, F.; Catelani, T.; Quarto, R.; Scaglione, S. Enhanced mechanical performances and bioactivity of cell laden-graphene oxide/alginate hydrogels open new scenario for articular tissue engineering applications. *Carbon* **2017**, *115*, 608−616.

(11) Wang, L.; Shelton, R. M.; Cooper, P. R.; Lawson, M.; Triffitt, J. T.; Barralet, J. E. Evaluation of sodium alginate for bone marrow cell tissue engineering. *Biomaterials* **2003**, *24*, 3475−3481.

(12) Kolambkar, Y. M.; Dupont, K. M.; Boerckel, J. D.; Huebsch, N.; Mooney, D. J.; Hutmacher, D. W.; Guldberg, R. E. An alginate based hybrid system for growth factor delivery in the functional repair of large bone defects. *Biomaterials* **2011**, *32*, 65−74.

(13) Fourest, E.; Volesky, B. Alginate properties and heavy metal biosorption by marine algae. *Appl. Biochem. Biotechnol.* **1997**, *67*, 215−226.

(14) Davis, T. A.; Volesky, B.; Mucci, A. A review of the biochemistry of heavy metal biosorption by brown algae. *Water Res.* **2003**, *37*, 4311−4330.

(15) Braccini, I.; Pérez, S. Molecular Basis of Ca^{2+}-Induced Gelation in Alginates and Pectins: The Egg-Box Model Revisited. *Biomacromolecules* **2001**, *2*, 1089−1096.

(16) Huang, X.; He, J.; Sun, K.; Chen, Y.; Zha, Z.; Zhou, C. Liquid crystal behavior and cytocompatibility of graphene oxide dispersed in sodium alginate solutions. *Carbon* **2018**, *129*, 258−269.

(17) Hu, X.; Tian, M.; Sun, B.; Qu, L.; Zhu, S.; Zhang, X. Hydrodynamic alignment and microfluidic spinning of strength-reinforced calcium alginate microfibers. *Mater. Lett.* **2018**, *230*, 148−151.

(18) Nagasawa, N.; Mitomo, H.; Yoshii, F.; Kume, T. Radiation-induced degradation of sodium alginate. *Polym. Degrad. Stab.* **2000**, *69*, 279−285.

(19) Zhou, Q.; Liu, Y.; Yu, G.; He, F.; Chen, K.; Xiao, D.; Zhao, X.; Feng, Y.; Li, J. Degradation kinetics of sodium alginate via sono-Fenton, photo-Fenton and sono-photo-Fenton methods in the presence of TiO_2 nanoparticles. *Polym. Degrad. Stab.* **2017**, *135*, 111−120.

(20) Primo, A.; Marino, T.; Corma, A.; Molinari, R.; García, H. Efficient visible-Light photocatalytic water splitting by minute amounts of gold supported on nanoparticulate CeO_2 obtained by a biopolymer templating method. *J. Am. Chem. Soc.* **2011**, *133*, 6930−6933.

(21) Hong, S.; Sycks, D.; Chan, H. F.; Lin, S.; Lopez, G. P.; Guilak, F.; Leong, K. W.; Zhao, X. 3D Printing of Highly Stretchable and Tough Hydrogels into Complex, Cellularized Structures. *Adv. Mater.* **2015**, *27*, 4035−4040.

(22) Zhao, H.-B.; Fu, Z.-B.; Chen, H.-B.; Zhong, M.-L.; Wang, C.-Y. Excellent electromagnetic absorption capability of Ni/Carbon based conductive and magnetic foams synthesized via a green one pot route. *ACS Appl. Mater. Interfaces* **2016**, *8*, 1468−1477.

(23) Gao, C.; Liu, M.; Chen, J.; Zhang, X. Preparation and controlled degradation of oxidized sodium alginate hydrogel. *Polym. Degrad. Stab.* **2009**, *94*, 1405−1410.

(24) Kong, H. J.; Kaigler, D.; Kim, K.; Mooney, D. J. Controlling rigidity and degradation of alginate hydrogels via molecular weight distribution. *Biomacromolecules* **2004**, *5*, 1720−1727.

(25) Kang, Y.-G.; Vu, H. C.; Le, T. T.; Chang, Y.-S. Activation of persulfate by a novel Fe(II)-immobilized chitosan/alginate composite for bisphenol A degradation. *Chem. Eng. J.* **2018**, *353*, 736−745.

(26) Abd El-Ghaffar, M. A.; Hashema, M. S.; El-Awadyb, M. K.; Rabiec, A. M. pH-sensitive sodium alginate hydrogels for riboflavin controlled release. *Carbohydr. Polym.* **2012**, *89*, 667−675.

(27) Fugetsu, B.; Satoh, S.; Shiba, T.; Mizutani, T.; Lin, Y.-B.; Terui, N.; Nodasaka, Y.; Sasa, K.; Shimizu, K.; Akasaka, T.; et al. Caged multiwalled carbon nanotubes as the adsorbents for affinity-based elimination of ionic dyes. *Environ. Sci. Technol.* **2004**, *38*, 6890−6896.

(28) Sa, V.; Kornev, K. G. A method for wet spinning of alginate fibers with a high concentration of single-walled carbon nanotubes. *Carbon* **2011**, *49*, 1859−1868.

(29) He, Y.; Zhang, N.; Gong, Q.; Qiu, H.; Wang, W.; Liu, Y.; Gao, J. Alginate/graphene oxide fibers with enhanced mechanical strength prepared by wet spinning. *Carbohydr. Polym.* **2012**, *88*, 1100−1108.

(30) Wang, X.-X.; Ma, T.; Shu, J.-C.; Cao, M.-S. Confinedly tailoring Fe_3O_4 clusters-NG to tune electromagnetic parameters and microwave absorption with broadened bandwidth. *Chem. Eng. J.* **2018**, *332*, 321−330.

(31) Lin, C.; Hu, L.; Cheng, C.; Sun, K.; Guo, X.; Shao, Q.; Li, J.; Wang, N.; Guo, Z. Nano-TiNb2O7/carbon nanotubes composite anode for enhanced lithium-ion storage. *Electrochim. Acta* **2018**, *260*, 65−72.

(32) Feng, A.; Jia, Z.; Zhao, Y.; Lv, H. Development of Fe/Fe3O4@C composite with excellent electromagnetic absorption performance. *J. Alloys Compd.* **2018**, *745*, 547−554.

(33) Yan, L.; Cao, L.; Dai, P.; Gu, X.; Liu, D.; Li, L.; Wang, Y.; Zhao, X. Metal-Organic Frameworks Derived Nanotube of Nickel−Cobalt

Bimetal Phosphides as Highly Efficient Electrocatalysts for Overall Water Splitting. *Adv. Funct. Mater.* **2017**, *27*, No. 1703455.
(34) Wang, Q.; Lei, Y.; Chen, Z.; Wu, N.; Wang, Y. B.; Wang, B.; Wang, Y. D. Fe/Fe3C@C nanoparticles encapsulated in N-doped graphene−MWCNTs framework as an efficient bifunctional oxygen electrocatalyst for robust rechargeable Zn−air batteries. *J. Mater. Chem. A* **2018**, *6*, 516−526.
(35) Li, Y.; Zhou, B.; Zheng, G.; Liu, X.; Li, T.; Yan, C.; Cheng, C.; Dai, K.; Liu, C.; Shen, C.; et al. Continuously prepared highly conductive and stretchable SWNT/MWNT synergistically composited electrospun thermoplastic polyurethane yarns for wearable sensing. *J. Mater. Chem. C* **2018**, *6*, 2258−2269.
(36) Dang, S.; Zhu, Q.-L.; Xu, Q. Nanomaterials derived from metal−organic frameworks. *Nat. Rev. Mater.* **2017**, *3*, No. 17075.
(37) Geng, P.; Zheng, S.; Tang, H.; Zhu, R.; Zhang, L.; Cao, S.; Xue, H.; Pang, H. Transition metal sulfides based on graphene for electrochemical energy storage. *Adv. Energy Mater.* **2018**, *8*, No. 1703259.
(38) Sheberla, D.; Bachman, J. C.; Elias, J. S.; Sun, C.-J.; Horn, Y. S.; Dincă, M. Conductive MOF electrodes for stable supercapacitors with high areal capacitance. *Nat. Mater.* **2017**, *16*, 220−225.
(39) Akasaka, T.; Watari, F. Capture of bacteria by flexible carbon nanotubes. *Acta Biomater.* **2009**, *5*, 607−612.
(40) Joddar, B.; Garcia, E.; Casas, A.; Stewart, C. M. Development of functionalized multi-walled carbon-nanotubebased alginate hydrogels for enabling biomimetic technologies. *Sci. Rep.* **2016**, *6*, No. 32456.
(41) Tsaih, M. L.; Chen, R. H. Effect of degree of deacetylation of chitosan on the kinetics of ultrasonic degradation of chitosan. *J. Appl. Polym. Sci.* **2003**, *90*, 3526−3531.
(42) Lutsyk, P.; Piryatinski, Y.; Shandura, M.; AlAraimi, M.; Tesa, M.; Arnaoutakis, G. E.; Melvin, A.; Kachkovsky, O.; Verbitsky, A.; Rozhin, A. Self-Assembly for Two Types of J-Aggregates: cis-Isomers of Dye on the Carbon Nanotube Surface and Free Aggregates of Dye trans-Isomers. *J. Phys. Chem. C* **2019**, *123*, 19903−19911.
(43) Pawar, S. N.; Edgar, K. J. Alginate derivatization: A review of chemistry, properties and applications. *Biomaterials* **2012**, *33*, 3279−3305.

https://doi.org/10.1021/acsomega.1c01159
ACS Omega 2021, 6, 12813−12819